nature geoscience

SUPPLEMENTARY INFORMATION
DOI: 10.1038/NGEO1686

Sea surface temperature in the north tropical Atlantic as a trigger for El Niño/Southern Oscillation events

Yoo-Geun Ham[1,2], Jong-Seong Kug[3], Jong-Yeon Park[3], and Fei-Fei Jin[4]

[1]Global Modeling and Assimilation Office, NASA/GSFC, Greenbelt, Maryland

[2]Goddard Earth Sciences Technology and Research Studies and Investigations, Universities Space Research Association

[3]Korea Institute of Ocean Science and Technology, Ansan, Korea

[4]Department of Meteorology, University of Hawaii, Honolulu, USA

Supporting Results

Observational analyses

Supplementary Fig. 1 shows the time series of DJF NINO3.4 SST from 1980 to 2010. To clarify the relationship between NTA SST and ENSO, years with NTA warming (NTA SST greater than one standard deviation) and cooling (NTA SST smaller than minus one standard deviation) during the previous FMA season are denoted by red and blue bars, respectively. There are six cases of NTA warming, and in each case a negative NINO3.4 SST followed. Similarly, three out of the four cases of NTA cooling show positive NINO3.4 SST during the following DJF season. These relationships imply that the NTA SST during the boreal spring season has a strong inverse relationship with the ENSO during the following winter season. Interestingly, three El Niño cases after

NTA cooling were in 1986/87, 1994/95, and 2009/10, which are warm-pool (WP) El Niño events[1] (also termed the dateline El Niño[2], El Niño Modoki[3], or central Pacific El Niño[4]) whose SST action centers are located over the central Pacific, which supports that the NTA cooling tends to enhance warming in the central Pacific, rather than in the eastern Pacific.

To investigate the oceanic response to the NTA-driven surface wind forcing, Supplementary Fig. 2 shows the regression of thermocline depth (using the 20^{o}C isotherm depth), and mixed-layer (using the top 50 m) current vectors. During the MAM season, the anticyclonic wind forcing over the subtropical eastern Pacific (Fig. 1a) tends to generate weak positive thermocline depth anomaly due to downwelling; however, it is not at the 95% confidence level in most of the regions. It implies that the off-equatorial pathway is mainly taken by the coupling between the mixed-layer SST and atmosphere without significant off-equatorial thermocline signals. The equatorial oceanic signals are also weak in the MAM season, indicating that there are weak preceding ENSO signals. During the JJA season, the thermocline depth and current anomalies are seen over the equatorial central Pacific between 180-120^{o}W due to the western Pacific easterly wind forcing. This negative thermocline depth signal is not extended to the eastern Pacific due to the local westerly wind forcing. During the SON season, the negative thermocline depth is stronger as the easterly wind forcing over the western Pacific is enhanced. It is interesting that the location of the largest negative thermocline depth anomaly is shifted about 30 degrees to the east of the location of the largest negative SST, suggesting that zonal advection is important for the central Pacific SST anomaly, as pointed out by a previous study[1].

Idealized experiment using CGCM

The role of the NTA as a trigger of the ENSO is also supported by idealized experiments using coupled general circulation model (CGCM)[5,6]. To separate the impact of NTA SST from other variabilities, two experiments are performed whose difference is only from the inclusion of the NTA warming. The experiment with positive NTA SST added to the climatological SST will be denoted as NTA experiment, while that with climatological SST is denoted as CTRL experiment. Supplementary Fig. 3 shows the prescribed SST anomalies used in NTA experiment. The magnitude of NTA SST is peak during boreal spring season. After the boreal spring season, the magnitude of the NTA SST gradually decreases, and almost disappears at boreal fall season.

The ensemble-mean differences in SST, precipitation, and wind vectors at 850hPa between NTA experiment from CTRL experiment is shown in Supplementary Fig. 4. During the MAM season, the NTA warming produces positive precipitation anomaly over the equatorial Atlantic. This atmospheric heating generates the cyclonic flow over the far-eastern Pacific, therefore, there is a resultant positive SST anomaly over the equatorial eastern Pacific by deepening the equatorial thermocline. At the same time, there is northerly over the off-equatorial central Pacific, and it is responsible for the local negative SST anomaly with reduced convective activity during JJA season. Then, this reduced convection generates equatorial easterly anomaly over the western Pacific as a part of the anticyclonic response, and it acts to induce the La Niña signal at subsequent season. Because the local westerly anomaly suppresses the development of La Niña signal over the far eastern Pacific, the maximum negative signal is shifted to the west as shown in observational analysis.

The oceanic response to the NTA-driven atmospheric wind forcing has been further examined (Supplementary Fig. 5). Consistent with the observation, the model result also shows there are competing processes between local westerly and remote easterly forcing in the eastern Pacific. That is, during the MAM season, the anomalous upwelling generated by the equatorial easterly appear in the central Pacific, while there are downwelling signals and related warming in the eastern Pacific due to the local westerlies as part of the cyclonic flow. The upwelling Kelvin-wave signal is generally extended toward the eastern Pacific in the following seasons to cool the eastern Pacific SST; however, the local westerlies directly induced by the NTA warming compensate this upwelling signal in the surface layer so that the subsurface temperature cannot develop in the far eastern Pacific.

Multi-model outputs in CMIP3 and CMIP 5

As shown earlier, it is suggested that the NTA SST tends to lead to larger SST anomalies over the central Pacific than over the eastern Pacific. Further analyses using multi-model outputs in the CMIP3 and CMIP5 support the results based on the observational data. The 18 and 23 CGCM simulations in the pre-industrial simulation participated in the CMIP3 and CMIP5 are also analyzed. Model references, details on the institutions where the models were run, and integration periods are summarized in Supp. Table 1. As they have the long-term simulations, the composite analyses may provide more robust results. The NTA warming (cooling) case is defined when NTA SST index is larger (smaller) than one (minus one) standard deviation during previous FMA season. To exclude the effect of ENSO signal in the previous year, the composite cases are further confined only when the magnitude of NINO3.4 SST during the previous DJF season is smaller than the 0.5 standard deviation. When all cases are used for the composites regardless of the ENSO state, the conclusion does not change.

Supplementary Fig. 6 shows the ENSO index (i.e., NINO3.4 SST) during the DJF season when there was significant NTA SST during previous FMA season. The multi-model ensemble (MME) of climate models shows clearly that the NTA SST warming and cooling during boreal spring followed by La Niña and El Niño at the 99%

confidence level, respectively. Among the 41 CMIP models, 31 models simulated El Niño after the NTA cooling, with only four producing La Niña. Similarly, 28 of the climate models simulated significant La Niña signal after the NTA warming, with only eight producing El Niño signal. These results support that the NTA SST during boreal spring is one of the important factors to initiate the ENSO.

In addition, to examine the role of NTA as a trigger in more detail, Supplementary Fig. 7 shows the ratio of El Niño, normal, La Niña events during the DJF season when an NTA SST event without ENSO event occurs during the previous FMA season. As it is defined as the ENSO event when it is over 0.5 standard deviation, the ratio for El Niño development would be 30% (denoted by black solid line) by assuming normal distribution if the NTA SST does not play any role. Consistent with the observational evidence, most of the models show that NTA cooling leads to a better chance for El Niño development in the subsequent winter. Although the onsets of El Niño and La Niña are largely determined by the residing ocean memories over the tropical Pacific as the ENSO theories suggest[7], the MME result indicates that 45% of NTA cooling cases lead to subsequent El Niño events, while only 17% of NTA cooling case is linked to subsequent La Niña events. This implies that the NTA SST can be one of the important components in triggering ENSO event.

How can these results be linked to the generation mechanism of the WP El Niño? To successfully simulate the role of NTA SST as a trigger of the WP El Niño, the model needs to simulate two types of El Niño independently. However, recent studies[8,9] reported that most state-of-the-art CGCMs have a serious problem in simulating two types of El Niño independently. In order to measure how well a climate model simulates the two types of El Niño, they[8,9] suggested to use the correlation coefficient between NINO3 index (150°W–90°W, 5°S–5°N) and NINO4 index (160°E–150°W, 5°S–5°N) during the DJF season of El Niño events in the CMIP archives. A lower correlation indicates more independent variation between NINO3 and NINO4 indices, so it might have a better simulation of the two types of El Niño. Note that the anomaly is defined as the deviation from the averaged Niño magnitude during the El Niño events[8,9]. The correlation in the CMIP models varies from -0.17 to 0.83, while the observed correlation is -0.28 from 1970 to 2009[9]. Based on this result, we select the 10 models whose correlation coefficients are close to the observed, which are CCCMA CGCM3.1, GFDL CM2.1, MIUB ECHO-g, and CNRM CM3 from the CMIP3, and CCSM4, CNRM CM5, FGOAL-S2, GFDL-ESM2M, GISS-E2-R, and INMCM4 from the CMIP5. Supplementary Fig. 8 shows the composite map of SST anomaly for the NTA cooling cases. Because the ENSO magnitude varies considerably among the models, composited SST anomaly is normalized by its temporal standard deviation before taking the multi-model ensemble. The criteria for the composite are the same as those used in Supplementary Fig. 6. From the JJA season, significantly positive SST anomalies are clearly seen over the equatorial Pacific. In both JJA and SON seasons, the maximum action center is located over the central Pacific between 170°E-160°W. Consistently, the magnitude of normalized SST anomaly over the NINO4 region is systematically larger than that over the NINO3 region, which implies that the spatial pattern of NTA-induced El Niño is the WP type.

In addition to being the effective trigger of the ENSO, our study also suggests that the NTA SST also can lead a fast phase transition of the ENSO[10], when ENSO events accompany NTA SST events[11]. To measure the impact of NTA SST on the ENSO transition, we firstly select El Niño (La Niña) events, which accompany the NTA warming (cooling) during following FMA(1) season. Then, we calculate the degree of the NINO3.4 transition as the difference of DJF NINO3.4 between two consecutive years [D(1)JF(2) NINO3.4 - D(0)JF(1) NINO3.4]. Supplementary Fig. 9 shows the difference in La Niña transition with and without the NTA cooling (or the difference in El Niño transition with and without the NTA warming) using the CMIP outputs. The result shows that the transition from the La Niña to the El Niño is faster when the NTA cooling occurs before the La Niña. Among the 41 CMIP models, 28 models show significantly faster transition from the La Niña to the El Niño when the NTA cooling accompanies the La Niña, while only two models simulate slower transition. Similarly, 38 of the climate models simulated significantly faster transition from the El Niño to the La Niña with the NTA warming, with only one model producing a slower transition.

Comparison with the role of Atlantic Niño

So far, several studies have examined impacts of Atlantic SST on the Pacific variability[10,12-16]. They mostly focused on the role of the Atlantic Niño, which is defined by the equatorially-averaged SST over the eastern Atlantic during boreal summer[15,17]. According to these studies, the Atlantic Niño can lead to La Niña signal during the subsequent winter season with a 6-month lag. To compare the role of Atlantic Niño to that of NTA SST, Supplementary Fig. 10 shows lag regression results using Atl3 index (20-0^{o}W, 3^{o}S-3^{o}N) during the JJA season. Consistent with previous studies, Atl3 is related to the subsequent La Niña event. However, there are some differences between NTA SST and Atlantic Niño.

One of the main differences is that the Atlantic Niño is likely to lead SST anomaly over the eastern Pacific[15], while NTA SST tends to lead SST anomaly over the central Pacific (Fig. 1c). This is because the westerly over the equatorial far-eastern Pacific is considerably weaker in the case of Atlantic Niño. For example, during the MAM season, the equatorial westerly over the far-eastern Pacific is hardly seen and confined over the western Atlantic Ocean in the case with the Atlantic Niño, while there is significant westerly extended to 160^{o}W in the case with the NTA SST (Fig. 1a). The equatorial westerly during the JJA season is also much weaker with the Atl3 index over the equatorial eastern Pacific. It means the thermocline deepening due to the equatorial westerly over the far-eastern Pacific is too weak to cancel the impact of equatorial easterly over the western Pacific in the case of Atlantic Niño. The other difference is that the wind anomaly is mainly over the equator in the case of Atlantic Niño, while the NTA SST affects the subtropical North Pacific variability. That is to say the Atlantic Niño modulates the ENSO through altering the Walker circulation, implying that the primary mechanism for the Atlantic Niño-induced Atlantic-Pacific connection is substantially different from that by the NTA SST, which affects the Pacific variability along the Pacific ITCZ.

Consistent with these differences between NTA SST and Atl3, the correlation coefficient between FMA NTA and JJA Atl3 indices is less than 0.1 during 1980 to 2010. In addition, the lead-lag correlation coefficients between FMA NTA SST and 3-month-moving-average Atlantic Niño index do not show any significant relation at the 95% significant level (less than 0.3 for the correlation), implying that they are independent precursors for the ENSO development to a large extent[18]. In addition, the year of the El Niño led by the Atlantic Niño is quite different from that led by the NTA SST. For example, the El Niño events in 1982/83 and 1997/98 were led by significantly (i.e., more than 1 standard deviation) negative Atl3, while the El Niño events in 1986/87, 1994/95, and 2009/10 were led by the NTA SST cooling. It further suggests that the Atlantic SST variability, including the Atlantic Niño and the NTA SST, is crucial for the (Pacific)

ENSO variability, and therefore careful monitoring and appropriate initialization of the tropical Atlantic Ocean may be essential for long-range ENSO forecasts.

References

1. Kug, J.-S., Jin, F.-F. & An, S.-I. Two types of El Niño events: Cold tongue El Niño and warm pool El Niño, *J. Clim*. **22**, 1499‑1515, doi:10.1175/2008JCLI2624.1 (2009).

2. Larkin, N. K. & Harrison, D. E. On the definition of El Niño and associated seasonal average U.S. weather anomalies. *Geophys. Res. Lett.* **32,** L13705, doi:10.1029/2005GL022738 (2005).

3. Ashok, K., Behera, S. K., Rao, S. A., Weng, H. & Yamagata, T. El Niño Modoki and its possible teleconnection, *J. Geophy. Res.* **112,** C11007, doi:10.1029/2006JC003798 (2007).

4. Kao, H.-Y. & Yu, J.-Y. Contrasting eastern-Pacific and central-Pacific types of ENSO. *J. Clim.* **22,** 615–632 (2009).

5. Griffies, S. M. *et al.* Formulation of an ocean model for global climate simulations. *Ocean Sci.*, **1**, 45-79 (2005).

6. Delworth, T. L. *et al.* GFDL's CM2 global coupled climate models. Part I: Formulation and simulation characteristics. *J. Clim*. **19,** 634-674 (2006).

7. Jin, F.-F. An equatorial ocean recharge paradigm for ENSO. Part I: Conceptual model. *J. Atmos. Sci.* **54**, 811–-829 (1997).

8. Ham Y. -G. & Kug, J.-S. How well do current climate models simulate two-types of El Niño? *Clim. Dyn.* doi:10.1007/s00382-011-1157-3 (2011).

9. Kug, J.-S. & Ham, Y. -G. Are there two types of La Niña? *Geophy. Res. Lett.* **38,** L16704, doi:10.1029/2011GL048237 (2011).

10. Dommenget, D., Semenov, V. & Latif, M. Impacts of the tropical Indian and Atlantic Oceans on ENSO. *Geophys. Res. Lett.* **33**, L11701, doi:10.1029/2006GL025871 (2006).

11. Alexander, M. A. & Scott, J. D. The influence of ENSO on air-sea interaction in the Atlantic, *Geophys. Res. Lett.* **29,** doi:10.1029/2001GL014347 (2002).

12. Dong, B.-W., Sutton R. T. & Scaife A. A. Multidecadal modulation of El Nio-Southern Oscillation (ENSO) variance by Atlantic Ocean Sea Surface Temperatures. *Geophys. Res. Lett*. **33**, L08705, doi:10.1029/2006GL025766 (2006).

13. Jansen, M. F., Dommenget, D. & Keenlyside, N. Tropical atmosphere–ocean interactions in a conceptual framework. *J. Clim.* **22,** 550–567 (2009).

14. Rodriguez-Fonseca, B. *et al.* Are Atlantic Niños enhancing Pacific ENSO events in recent decades? *Geophys. Res. Lett.* **36,** L20705. DOI: 10.1029/2009GL040048 (2009).

15. Ding, H., Keenlyside, N. S. & Latif, M. Impact of the Equatorial Atlantic on the El Niño Southern Oscillation. *Clim. Dyn.* **38,** 1965-1972, doi:10.1007/s00382-011-1097-y (2011).

16. Frauen, C. & Dommenget D. Influences of the tropical Indian and Atlantic Oceans on the predictability of ENSO, *Geophys. Res. Lett*. **39**, L02706, doi:10.1029/2011GL050520 (2012).

17. Keenlyside, N. S. & Latif, M. Understanding equatorial Atlantic interannual variability. *J. Clim.* **20,** 131–142 (2007).

18. Servain, J., Wainer, I., McCreary, J. P. & Dessier A. Relationship between the equatorial and meridional modes of climatic variability in the tropical Atlantic. *Geophys. Res. Lett*., **26(4)**, 485488, doi:10.1029/1999GL900014 (1999).

Archive	Modeling Group	Model Number	CMIP ID	Integration period
CMIP3	BCCR	**1**	**BCCR-BCM2.0**	250 year
	CCCMA	**2**	**CCCMA_CGCM_3.1**	500 year
	CCCMA	**3**	**CCCMA_CGCM_3.1_t63**	400 year
	Météo-France	**4**	**CNRM-CM3**	500 year
	CSIRO Atmospheric Research	**5**	**CSIRO-Mk3.0**	380 year
		6	**CSIRO-Mk3.5**	500 year
	NOAA / GFDL	**7**	**GFDL-CM2.0**	500 year
		8	**GFDL-CM2.1**	500 year
	LASG	**9**	**IAP_FGOALS-g1.0**	150 year
	INGV	**10**	**INGV_ECHAM4**	100 year
	INM	**11**	**INM-CM3.0**	330 year
	IPSL	**12**	**IPSL-CM4**	500 year
	CCSR, JAMSTEC	**13**	**MIROC3.2_HIRES**	100 year
		14	**MIROC3.2_MEDRES**	500 year
	University of Bonn, KMA	**15**	**MIUB_ECHO-G**	340 year
	MRI	**16**	**MRI-CGCM2.3.2a**	350 year
	Hadley Centre /Met Office	**17**	**UKMO-HadCM3**	250 year
		18	**UKMO-HadGEM1**	230 year
CMIP5	BCCR	**19**	**BCC-CSM1.1**	500 year
	NCAR	**20**	**CCSM4**	500 year
	Météo-France	**21**	**CNRM-CM5**	850 year
	CSIRO	**22**	**CSIRO-Mk3-6-0**	500year
	LASG	**23**	**FGOALS-g2**	500 year
		24	**FGOALS-s2**	700 year
	NOAA / GFDL	**25**	**GFDL-ESM2G**	500 year
		26	**GFDL-ESM2M**	500 year
		27	**GFDL-CM3**	500 year
	NASA / GISS	**28**	**GISS-E2-H**	480 year
		29	**GISS-E2-R**	850 year
	Hadley Centre / Met Office	**30**	**HadGEM2-CC**	240 year
		31	**HadGEM2-ES**	480 year
	INM	**32**	**INM-CM4**	500 year
	IPSL	**33**	**IPSL-CM5A-LR**	1000 year
		34	**IPSL-CM5A-MR**	1000 year
	CCSR, JAMSTEC	**35**	**MIROC4h**	100 year
		36	**MIROC5**	670 year
		37	**MIROC-ESM**	530 year
	MPI-M	**38**	**MPI-ESM-LR**	1000 year
		39	**MPI-ESM-P**	1000 year
	MRI	**40**	**MRI-CGCM3**	500 year
	NCC	**41**	**NorESM1-M**	500 year

Supplementary Table 1. Description of the models from the CMIP archives.

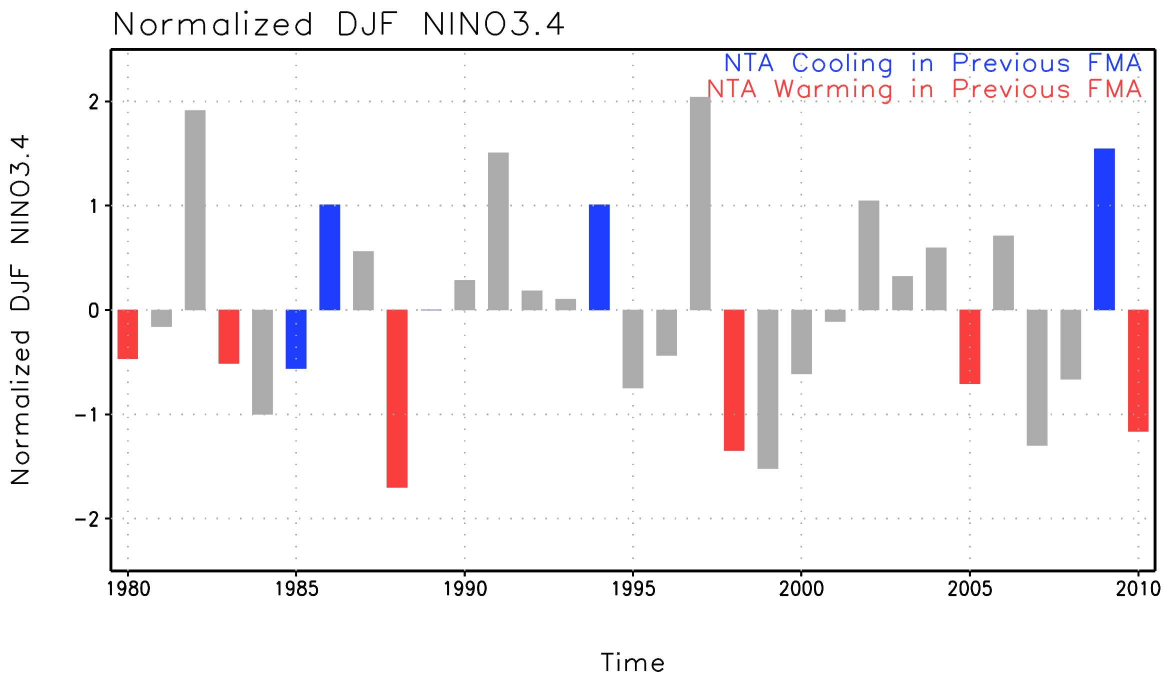

Supplementary Figure 1. Time series of DJF NINO3.4 SST from 1980 to 2010. Note that the years with NTA warming (NTA SST greater than one standard deviation) and cooling (NTA SST smaller than negative one standard deviation) during the previous FMA season are denoted by red and blue bars, respectively.

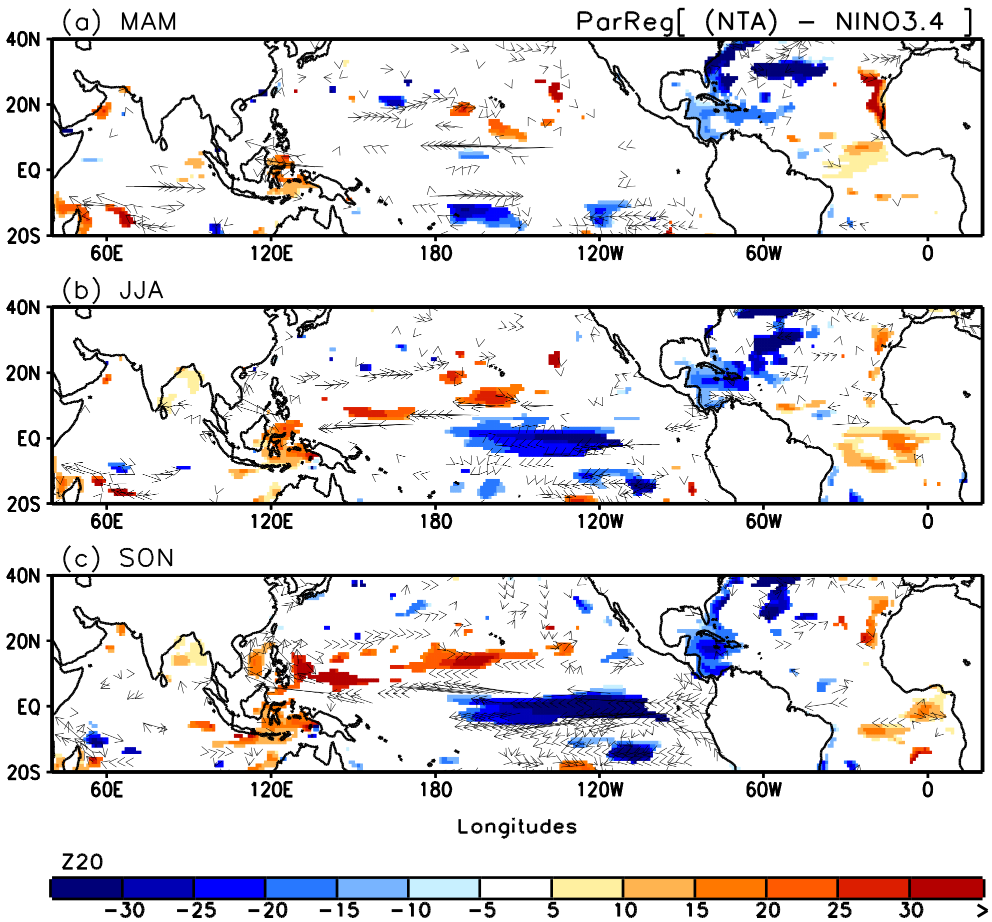

Supplementary Figure 2. Lagged regressions between the NTA index during the FMA season and thermocline depth (using the 20^{o}C isotherm depth), and mixed-layer (using top 50 m) current vectors during (a) MAM, (b) JJA, and (c) SON seasons, after excluding the impact of NINO3.4 SST during the previous DJF season. Only the values at the 95% confidence level or higher are shown.

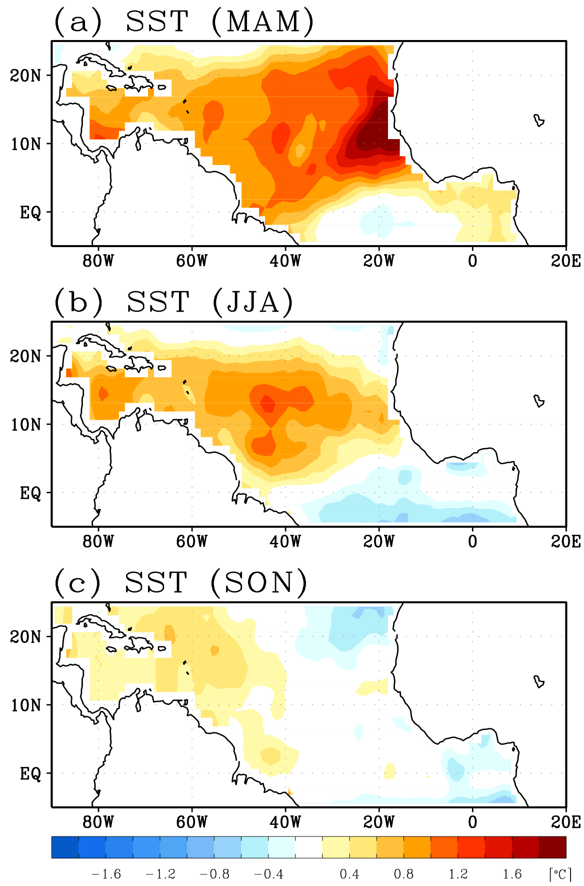

Supplementary Figure 3. The prescribed SST anomalies for NTA experiment.

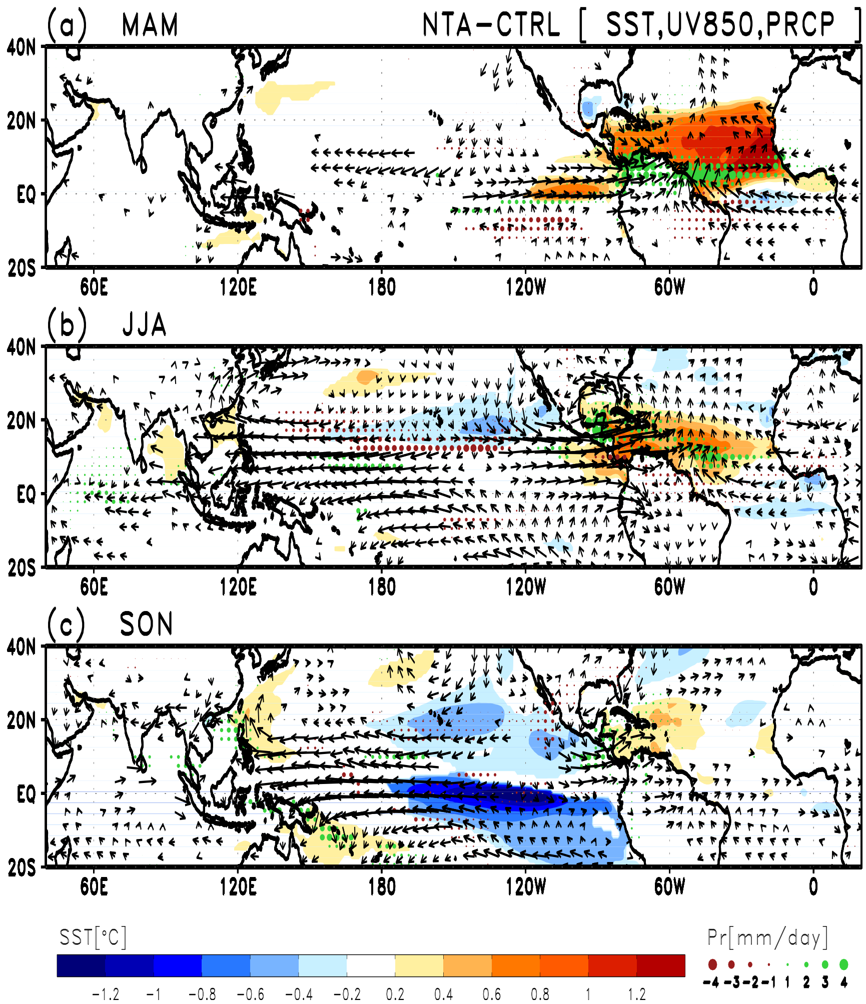

Supplementary Figure 4. The ensemble-mean differences in SST, precipitation, and wind vector at 850 hPa between NTA experiment from CTRL experiment during the (a) MAM, (b) JJA, and (c) SON season. The values over 95% confidence level is only drawn.

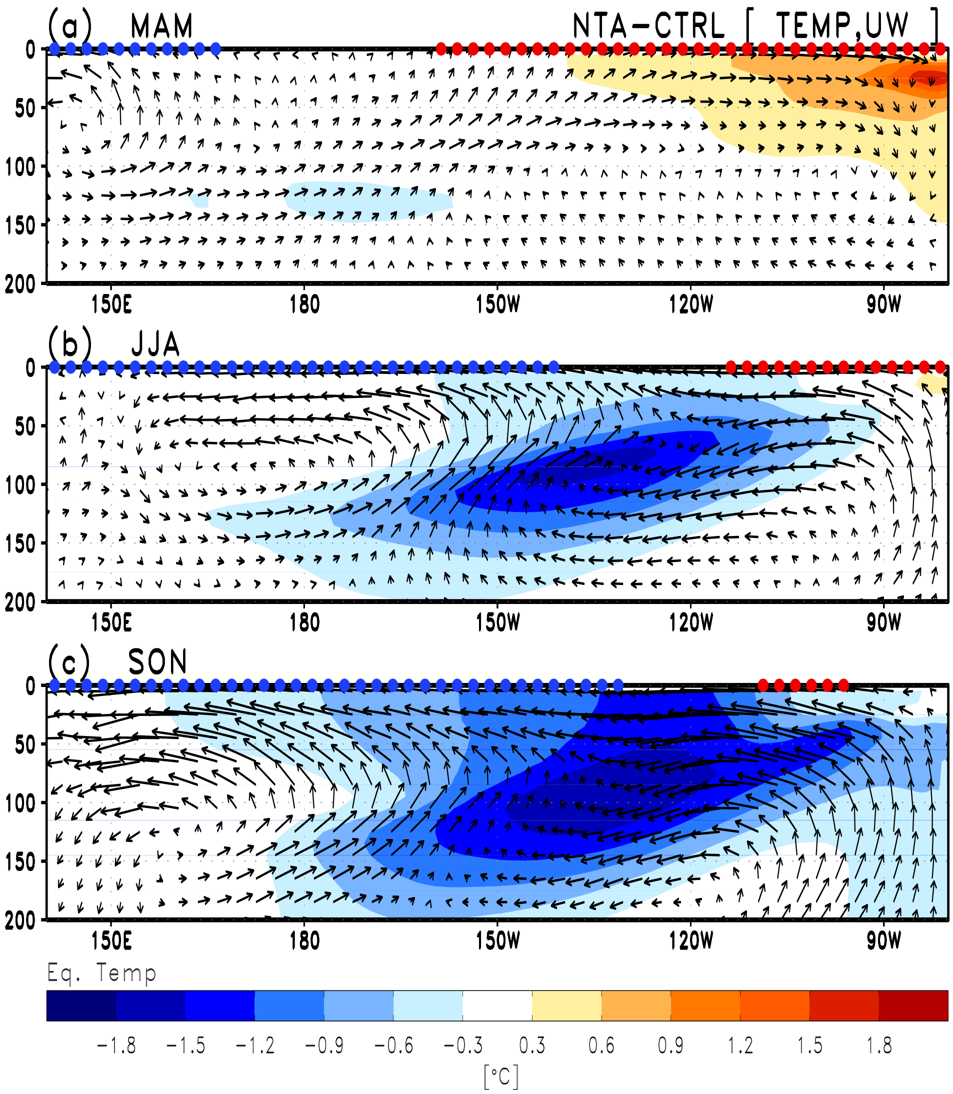

Supplementary Figure 5. Ensemble-mean difference of equatorial (2°S-2°N) subsurface temperature, oceanic zonal currents, and vertical velocities during (a) MAM, (b) JJA, and (c) SON seasons between the NTA experiment and CTRL experiment. The red and blue dots at the surface layer are marked when there are positive (negative) 850-hPa zonal wind anomalies above 0.4 m/s (below -0.4 m/s).

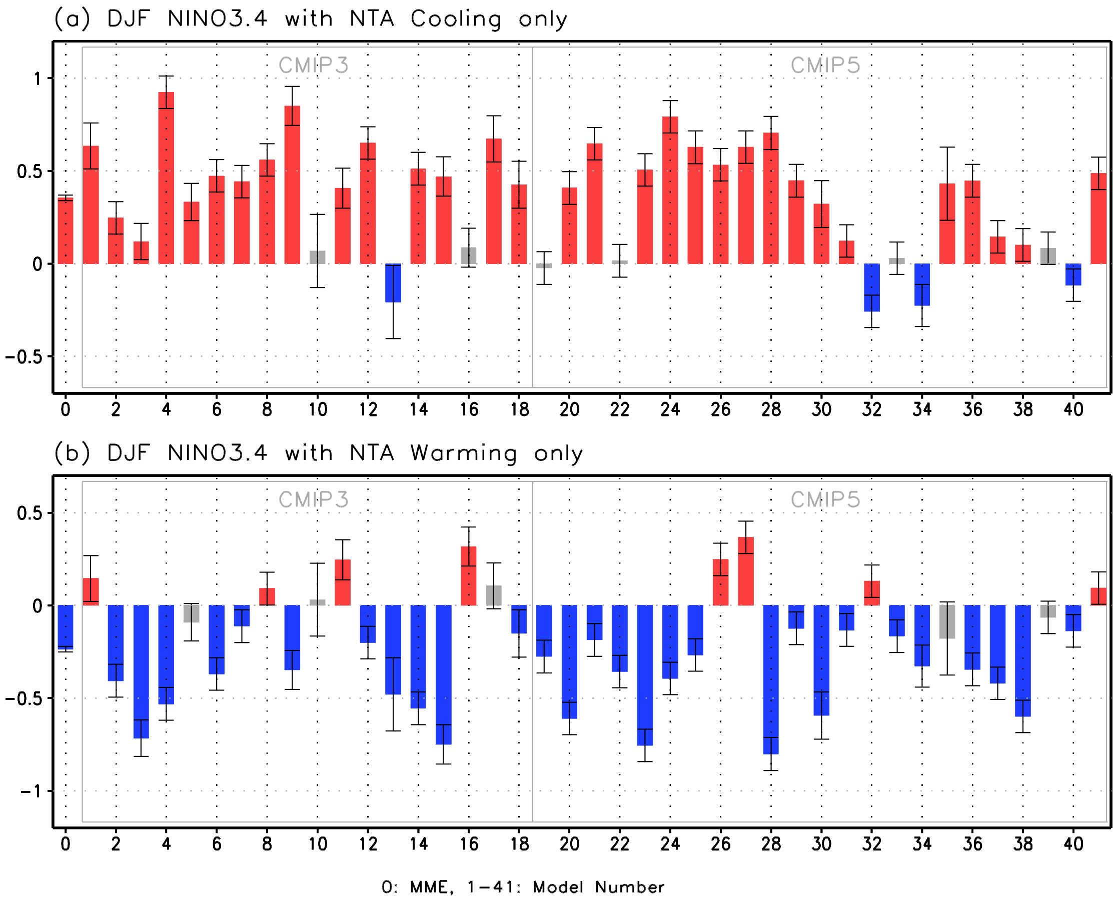

Supplementary Figure 6. The magnitude of NINO3.4 SST during DJF season with significant NTA SST (i.e., larger than one standard deviation) during the previous FMA season participated in the Coupled Model Intercomparison Project Phases 3 and 5 (CMIP3 and CMIP5). Note that the cases are selected only when the magnitude of NINO3.4 SST during the previous DJF season is smaller than 0.5 standard deviation, in order to exclude the ENSO signal in the previous year. The number 0 in the x-axis denotes Multi-Model Ensemble (MME), and numbers 1-41 denote individual climate models.

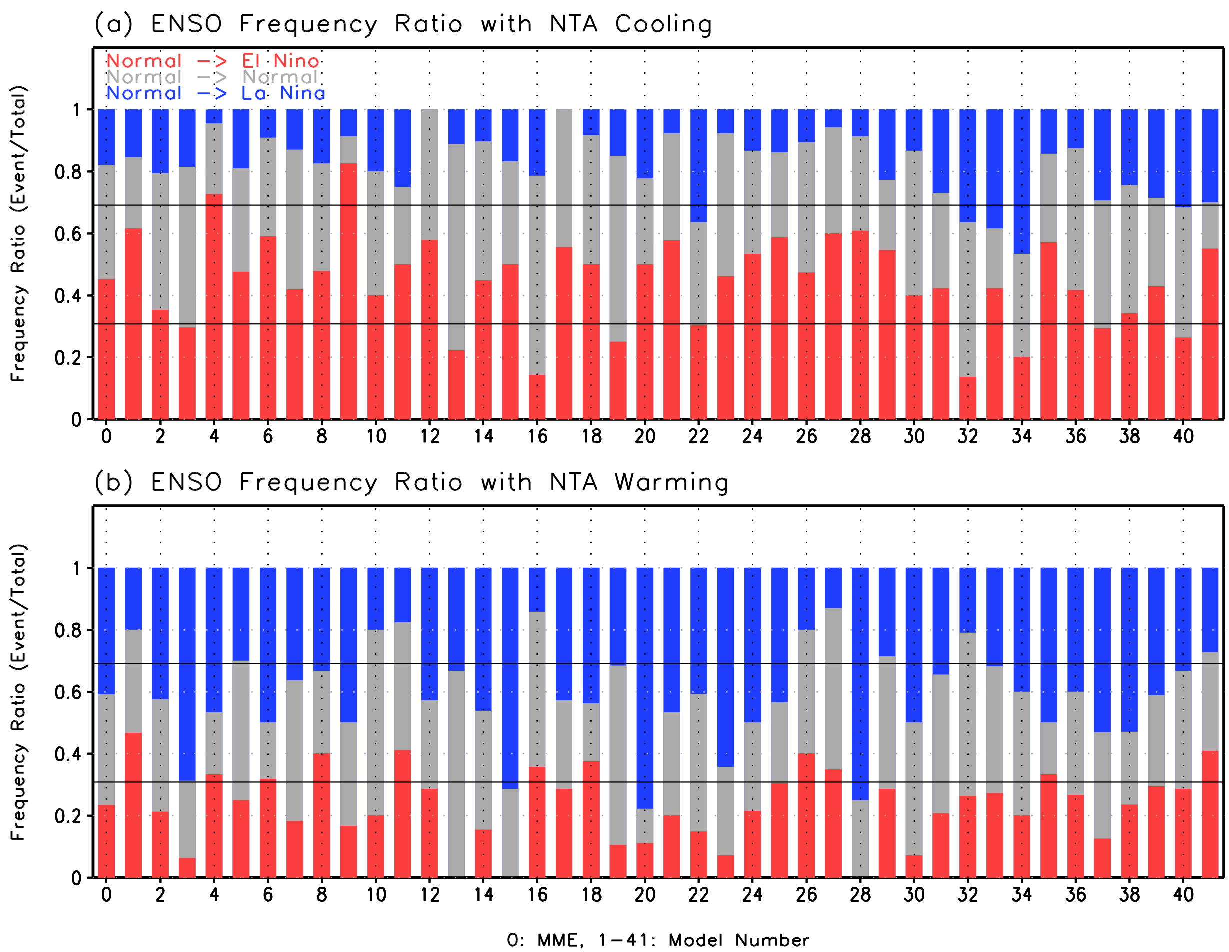

Supplementary Figure 7. (a) The ratio of El Niño, normal, La Niña events during the following DJF season when the NTA SST cooling during the FMA occurs without ENSO events. (b) Same as (a), but for the NTA warming case.

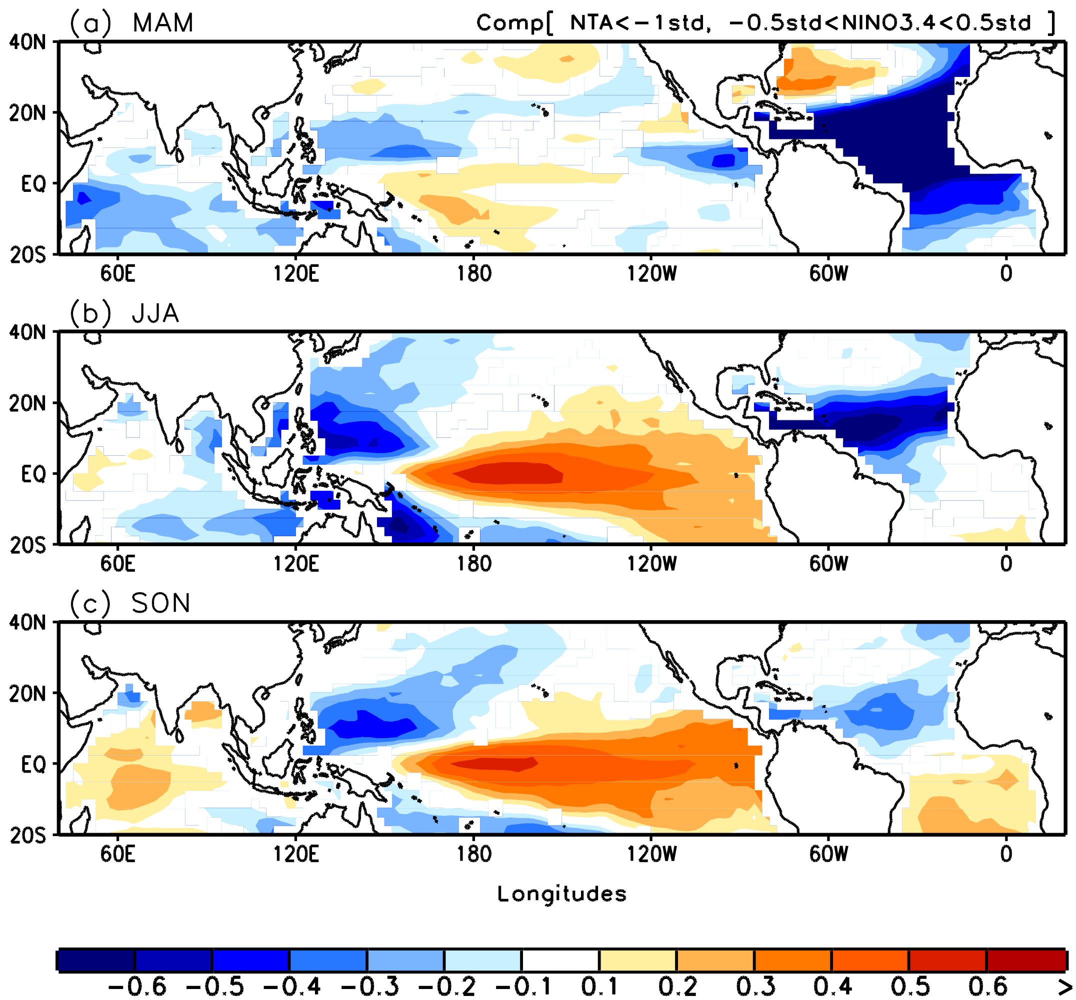

Supplementary Figure 8. Composite of normalized SST anomalies from 10 CMIP models (i.e., CCCMA CGCM 3.1-t63, GFDL CM2.1, MIUB ECHO-g, and CNRM CM3 from the CMIP3, and CCSM4, CNRM CM5, FGOAL-S2, GFDL-ESM2M, GISS-E2-R, and INMCM4 from the CMIP5) when there is a significant NTA cooling during the FMA season. Note that the criteria for the composite are the same as those used in Fig. 4.

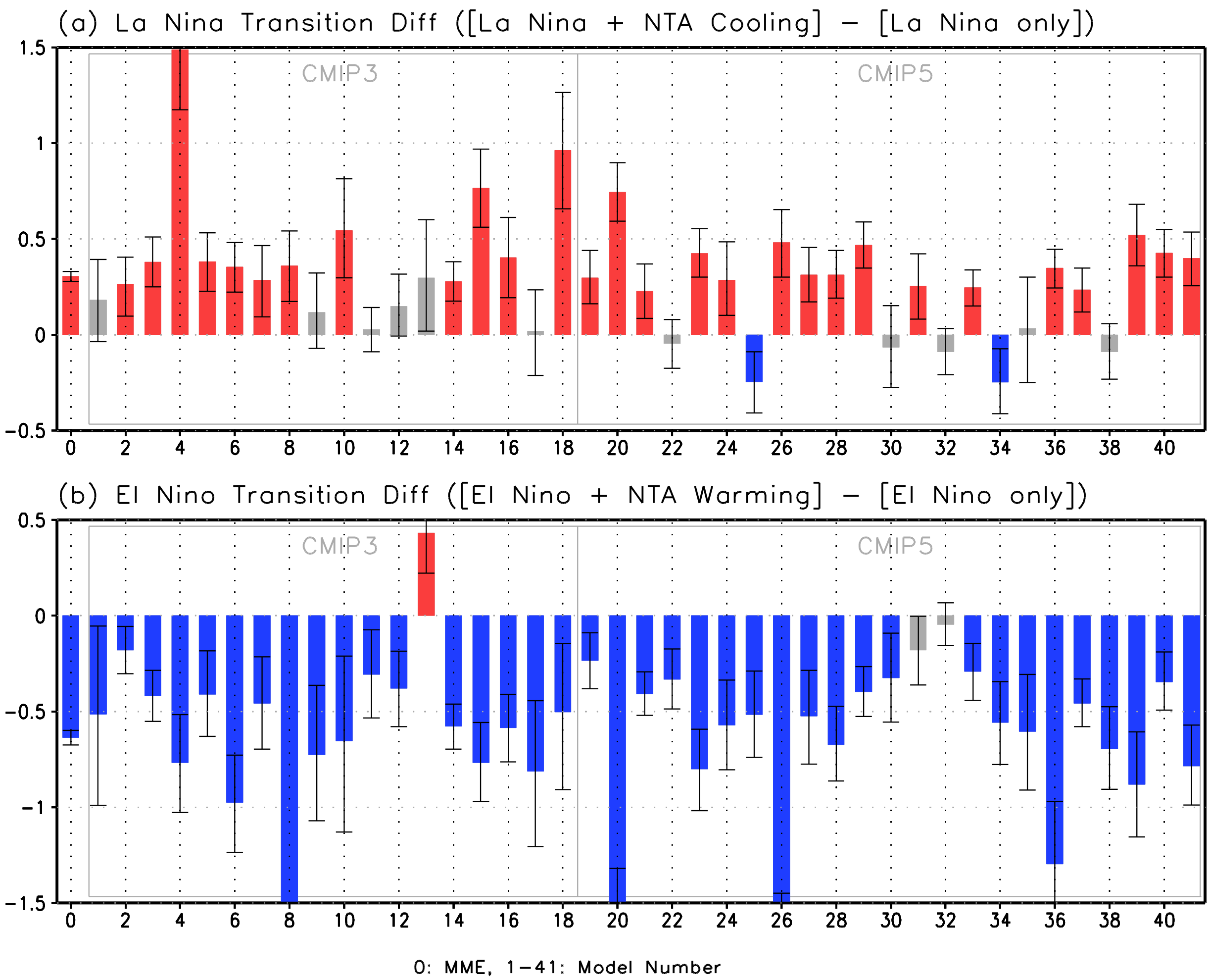

Supplementary Figure 9. (a) The difference of La Niña transition with significant (larger than one standard deviation) NTA cooling from that without the NTA cooling in the CMIP3 and CMIP5. (b) Same as (a), but for El Niño. The number 0 in the x-axis denotes MME, and numbers 1-41 denote individual climate models.

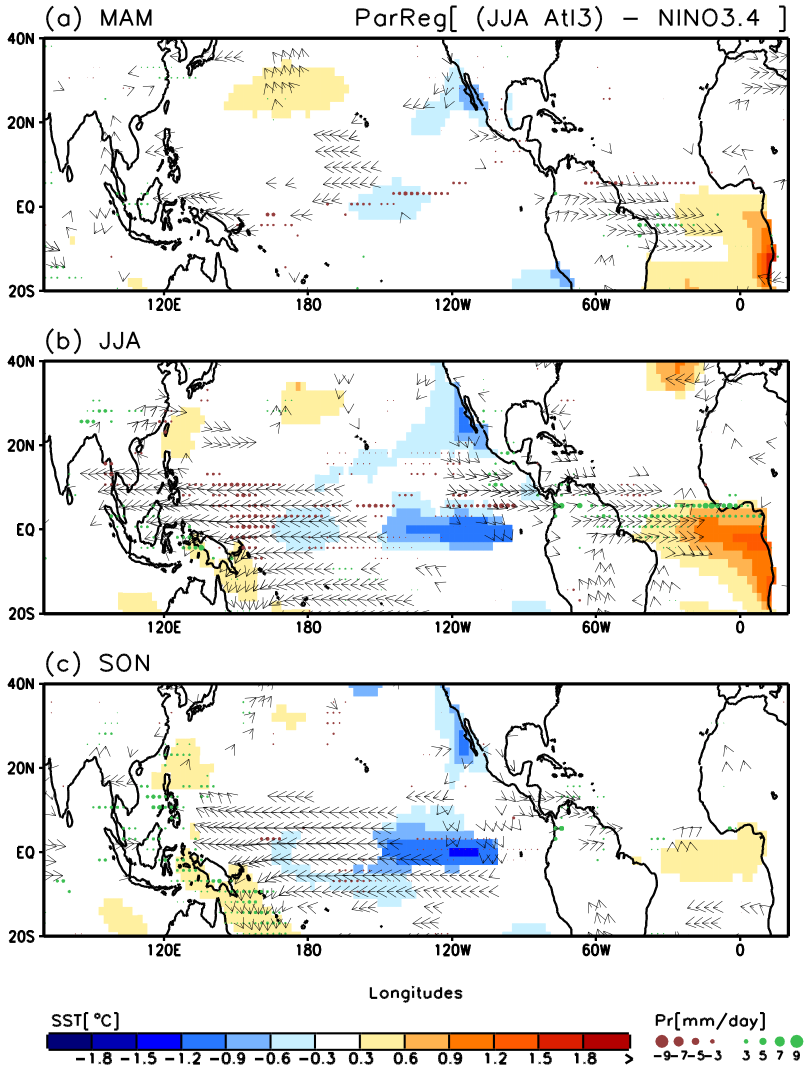

Supplementary Figure 10. Lagged regressions between the Atl3 index (20-0°W, 3°S-3°N) averaged during the JJA season and SST, wind vector at 850hPa (vector), and precipitation during (a) MAM, (b) JJA, and (c) SON seasons, after excluding the impact of NINO3.4 SST (170-120°W, 5°S-5°N) during the previous DJF season. Only the values at the 95% confidence level or higher are shown.